

Analytical model for photoluminescence quenching via Förster resonant energy transfer in a conjugated polymer doped by energy acceptors

S. A. Zapunidi, Yu. V. Krylova, and D. Yu. Paraschuk

International Laser Center and Faculty of Physics, M.V. Lomonosov Moscow State University, 119991 Moscow, Russia

(Received 30 August 2008; revised manuscript received 5 April 2009; published 15 May 2009)

An analytical model of quenching of steady-state photoluminescence (PL) via Förster resonant energy transfer (FRET) in blends of a conjugated polymer and low-molecular energy acceptors is presented. The normalized PL intensity as an analytical function of acceptor concentration is obtained in the case of homogeneous polymer-acceptor blend. This function has only two parameters depending on the Förster radii of energy transfer between the polymer conjugated segments (intrapolymer) and between a conjugated segment and an energy acceptor. The intrapolymer exciton migration can enhance PL quenching up to 60% as derived as an asymptote of the model. The model excellently fits the experimental data on quenching of soluble polyphenylenevinylene PL in blends with trinitrofluorenone.

DOI: [10.1103/PhysRevB.79.205208](https://doi.org/10.1103/PhysRevB.79.205208)

PACS number(s): 78.20.Bh, 78.55.Kz, 78.66.Qn

I. INTRODUCTION

Conjugated polymers are actively studied nowadays to be used in various organic devices such as light emission diodes (LEDs) and solar cells. The processes of generation, transport, recombination, and dissociation of excitons, which are considered as the lowest energy excitations in conjugated polymers, are of key importance for the device performance. In polymer solar cells, excitons are generated by light absorption and their further dissociation results in separated electron-hole pairs. In polymer LEDs, excitons are formed after injection of electrons and holes from the cathode and anode, respectively, resulting in luminescence.

Exciton dynamics in conjugated polymers is commonly probed by photoluminescence (PL), e.g., exciton dissociation results in quenching of the polymer PL. PL quenching mechanisms in conjugated polymers could be divided into two groups: dependent and independent on the photoexcitation intensity. The former group is related to singlet-triplet annihilation,¹ singlet-singlet annihilation,^{2,3} and quenching by free charges.^{4,5} These mechanisms are associated with interaction between excitons or between an exciton and a charge generated from another exciton. The latter group is related to quenching by electric field,⁶⁻⁹ intersystem crossing,¹⁰ charge transfer to an electron acceptor,¹¹ and Förster resonant energy transfer (FRET) to an energy acceptor.¹²⁻¹⁴

At low photoexcitation intensity ~ 100 mW/cm², i.e., about the sun one on the Earth's surface, the intensity independent mechanisms seem to be dominant in the PL quenching. In polymer solar cells, excitons must dissociate into free electron-hole pairs with high probability in comparison to other concurring processes, e.g., PL. Efficient exciton dissociation (photoinduced charge transfer) is realized in blends of conjugated polymers with electronic acceptors, specifically fullerenes. At the same time, in widely studied blends of polyphenylenevinylene and fullerene derivatives, the fullerene can also be an efficient energy acceptor providing efficient FRET from the polymer to the fullerene.¹⁵ Moreover, FRET could also be efficient in those donor-acceptor blends where the polymer forms a ground-state charge-

transfer complex with an electron acceptor molecule.^{16,17} In fact, if such a complex has intense absorption in the spectral region of the polymer PL,^{16,17} the FRET from the uncomplexed polymer segments to the complex is expected. Thus, both photoinduced charge transfer and FRET can result in efficient PL quenching in blends of luminescent conjugated polymers with electronic acceptors.

If the energy acceptor is highly luminescent, the FRET efficiency in the polymer-acceptor blend could be determined from PL of both the polymer and the acceptor.¹⁴ If the quantum yield of acceptor PL is low, e.g., as in fullerenes, the acceptor induced PL quenching stemming from either/both energy or/and charge transfer can be easily studied by measuring the dependence of the polymer PL on the acceptor concentration under continuous-wave (cw) photoexcitation. Photoexcitation in the cw mode allows using low photoexcitation intensities to avoid the intensity-dependent PL quenching processes. This PL quenching curve can be measured in a wide dynamic range amounting three orders of magnitude and more in PL intensity and then be fitted by a model describing the most significant PL quenching processes.

The well-known PL quenching models for low-molecular-weight donor-acceptor blends^{13,18} do not take into account the multichromophoric structure of conjugated polymers, which includes conjugated segments of various optical gaps. It is believed that photoexcitation of the conjugated polymer leads to efficient energy transfer from shorter conjugated segments to the longer ones resulting in efficient exciton migration. Taking into account these intrapolymer energy transfers, Arkhipov *et al.* suggested in Ref. 12 a model describing PL quenching of a conjugated polymer doped by an energy acceptor. The authors calculated the kinetics of the polymer PL for different acceptor concentration. The PL quenching curve in the cw mode can be derived via numerical integration of the model and is described by four parameters.¹²

In this work, we present an analytical model describing migration and quenching of excitons via FRET in blends of a conjugated polymer and an energy acceptor. The steady-state energy distribution of excitons is found by solving the balance equation taking into account their photogeneration, re-

combination, and both intrapolymer and polymer-acceptor FRETs. The spatial migration of excitons is taken into account by the introduction of their quenching rate distribution. We apply our model to the simplest case of randomly distributed acceptor molecules in the polymer and derive a two-parameter analytical dependence of the polymer cw PL on the acceptor concentration. Then, we compare the model with the experimental data in blends of soluble polyphenylenevinylenes and a low-molecular-weight acceptor. Finally, assumptions, useful asymptotes, and possible extensions of the model are discussed.

II. MODEL

A. Model approach

The FRET results from the dipole-dipole interaction between an energy donor and energy acceptor. The FRET rate depends on their spectral properties, orientation of the transition dipole moments, and distance r (Ref. 19),

$$\nu(r) = \frac{9000 \cdot \ln 10 \cdot k^2}{\tau \cdot 128 \cdot \pi^6 \cdot n^4 \cdot N_A \cdot r^6} \int_0^\infty p_D(f) \cdot \varepsilon_A(f) \cdot \frac{df}{f^4}, \quad (1)$$

where τ is the radiative lifetime of the excited donor (conjugated polymer segment), n is the refraction index, N_A is Avogadro's number, $\varepsilon_A(f)$ is the acceptor molar decadic extinction, $p_D(f)$ is the donor area-normalized luminescence spectrum, and k is the orientation parameter equal to $2/3$ for the random orientation of the donor and acceptor transition dipole moments. The distance at which the FRET rate equals the luminescence rate is defined as the Förster radius,

$$r_F^6 = \frac{9000 \cdot \ln 10 \cdot k^2}{128 \cdot \pi^6 \cdot n^4 \cdot N_A} \int_0^\infty p_D(f) \cdot \varepsilon_A(f) \cdot \frac{df}{f^4}. \quad (2)$$

If the PL and absorption spectra of individual molecules are used in Eq. (2), it gives a complete description of FRET specifically for ladder-type polyphenylene single chains.²⁰ However, in the case of inhomogeneous spectral broadening typical for conjugated polymers, spectra of individual chromophores and luminophores are usually not directly accessible from experiment, and one has to use ensemble-averaged spectra in Eq. (2). As a result, Eq. (2) gives an effective r_F without correct temperature dependence of FRET. The latter can be introduced in a model assuming that FRETs to the lower energy states ($E_A \leq E_D$) is always available, while the FRET rate to the higher energy states ($E_A > E_D$) is described by the Boltzmann distribution.^{12,21} Then, from Eqs. (1) and (2) we have

$$\nu(E_D, E_A, r, T) = \frac{1}{\tau} \cdot \left(\frac{r_F}{r}\right)^6 \cdot \begin{cases} 1, & E_A \leq E_D \\ \exp\left(-\frac{E_A - E_D}{k_b T}\right), & E_A > E_D. \end{cases} \quad (3)$$

Equation (3) defines the FRET rate from donor D with

energy E_D to acceptor A with energy E_A at temperature T , k_b is the Boltzmann constant.

We will consider two types of FRETs in blends of a conjugated polymer and energy acceptors: between its conjugated segments (intrapolymer) and from a conjugated segment to the acceptor. Energy transfer from a donor (conjugated segment) to an acceptor results in PL quenching because the transferred excitation cannot be transferred back to the polymer and hence contribute to PL. FRET between conjugated segments results in energy relaxation and spatial migration of excitons. To describe the FRET, we will use distributions of excitons in energy and in quenching rate. The quenching rate characterizes the exciton spatial position relative to the energy acceptors. By adding the quenching rate as a new variable one can distinguish the excitons located at different distances from the acceptors and take into account spatial exciton migration through the conjugated segments during FRET.

To describe PL quenching in our model, we need a number of assumptions: (i) The polymer-acceptor blended films are thick enough to neglect any interface effects and thin enough to avoid PL reabsorption. This condition is generally fulfilled in films with thickness in the range ~ 20 – 200 nm. (ii) Photoexcitation is monochromatic and all conjugated segments of the polymer have the same absorption cross-section at the photoexcitation wavelength. (iii) Intensity-dependent PL quenching is neglected. (iv) The temperature influence on the FRET is low enough, i.e., exciton migration in energy is unidirectional from the higher energies to the lower ones according to Eq. (3). (v) The PL and nonradiative transition rates of excitons are energy independent, with the vibrational relaxation rate being much higher. (vi) FRET occurs between pointlike donors and acceptors, i.e., exciton delocalization along the conjugated segments is not taken into account. Apart from these approximations, we will use the minimum donor-acceptor distance r_{\min} limited by their sizes. Finally, we will approximate Förster radii by two ones: between conjugated segments and between a conjugated segment and an energy acceptor. These assumptions will be discussed below in Sec. IV.

In the model, we use a quenching rate ν as an independent variable characterizing an exciton. This rate can map the spatial position of each exciton relative to the quenchers. As a result, exciton spatial migration can now be described via a variation in ν . Suppose that quenchers are somewhat spatially distributed in the sample. For an exciton generated at any point in the sample, we can assign a certain quenching rate that will depend on the distances to the quenchers. As a result, the exciton can be characterized by a distribution on exciton quenching rates $P(\nu)$ that depends both on the acceptor spatial distribution and the specific quenching mechanism. The explicit form of $P(\nu)$ for the random distribution of quenchers and Förster quenching mechanism will be given later.

Consider the processes determining the number and properties of the singlet excitons and write down a steady-state balance equation for their distribution in energy and quenching rates $N(E, \nu)$,

$$\begin{aligned} \frac{\partial N(E, \nu)}{\partial t} = & \frac{G}{n} \cdot g(E) \cdot P(\nu) - N(E, \nu) \left(\frac{1}{\tau} + \frac{1}{\tau_R} \right) - \frac{N(E, \nu) \cdot r_i^6 \cdot 4\pi}{3 \cdot \tau \cdot r_{\min}^3} \int_0^E g(E_A) dE_A \\ & + \frac{g(E) \cdot r_i^6 \cdot 4\pi \cdot P(\nu)}{3 \cdot \tau \cdot r_{\min}^3} \cdot \int_E^\infty \left(\int_0^\infty N(E_D, \bar{\nu}) d\bar{\nu} \right) dE_D - N(E, \nu) \cdot \nu. \end{aligned} \quad (4)$$

Here, the first term in the RHS describes photogeneration of excitons with the photon absorption rate G at conjugated segments with the concentration $g(E)$, with their total concentration being $n = \int_0^\infty g(E_D) dE_D$. The second term takes into account exciton radiative and nonradiative relaxation with characteristic times τ and τ_R , correspondingly. The third and fourth terms in the RHS of Eq. (4) characterize FRET to lower energy and from higher energy conjugated segments, respectively; these terms are discussed below. The last term in Eq. (4) describes exciton quenching via FRET to an energy acceptor. According to the definition of ν , the quenching by acceptors is energy independent and determined solely by ν .

We describe intrapolymer energy transfer as the disappearance of an exciton with parameters (E_1, ν_1) and the appearance of an exciton with parameters (E_2, ν_2) . The condition $E_2 \leq E_1$ limits the available FRET routes.

The disappearance of excitons with parameters (E, ν) is described by the third term in the RHS of Eq. (4). The disappearance rate depends on the number of these excitons and the FRET rate [Eq. (3)] integrated over the available energies $[0, E]$ and coordinates $[r_{\min}, \infty]$,

$$\begin{aligned} \left. \frac{\partial N(E, \nu)}{\partial t} \right|_{\text{FRET}(-)} = & -N(E, \nu) \cdot \int_{r_{\min}}^\infty \\ & \times 4\pi r^2 \int_0^E g(E_A) \cdot \nu(E, E_A, r, T) dE_A dr, \end{aligned} \quad (5)$$

where r_{\min} is the minimal distance between conjugated segments. Substituting $\nu(E, E_A, r, T)$ in Eq. (5) for Eq. (3) and denoting the Forster radius as r_i , we get the third term in the RHS of Eq. (4).

FRET from higher energy segments results in excitons appearing at lower energy segments. The number of higher energy excitons generating an exciton with energy E , given by the fourth term in the RHS of Eq. (4), is obtained from the integrated over ν exciton distribution $N(E, \nu)$, multiplied by the FRET rate [Eq. (3)], and integrated over all energies higher than E . Multiplying the result by the concentration of conjugated segments with energy E and integrating the product over space we get

$$\begin{aligned} \left. \frac{\partial N(E)}{\partial t} \right|_{\text{FRET}(+)} = & \int_{r_{\min}}^\infty g(E) \cdot 4\pi r^2 \int_E^\infty \\ & \times \left[\int_0^\infty N(E_D, \bar{\nu}) d\bar{\nu} \right] \cdot \nu(E_D, E, r, T) dE_D dr. \end{aligned} \quad (6)$$

Now we need to find the quenching rate ν of the appeared

exciton. Assume that the exciton appears at a random point in space and its quenching rate does not depend on the former one, i.e., it is determined solely by the function $P(\nu)$,

$$\left. \frac{\partial N(E, \nu)}{\partial t} \right|_{\text{FRET}(+)} = P(\nu) \left. \frac{\partial N(E)}{\partial t} \right|_{\text{FRET}(+)}. \quad (7)$$

This is evidently true for the homogeneous acceptor distribution. In the case of inhomogeneous acceptor distribution this assumption is true if the characteristic distance of FRET is higher than the characteristic length of acceptor inhomogeneity, e.g., its aggregation. Combining Eqs. (3), (6), and (7), we get the fourth term in the RHS of Eq. (4) that describes FRET from the higher energy segments.

B. Balance equation

We have taken into account all the processes determining the exciton kinetics within our model. Consider the steady-state case in which the appearance of excitons of a given energy and quenching rate is balanced with their disappearance. Equating the LHS of Eq. (4) to zero, we get

$$\begin{aligned} g(E)P(\nu) \left\{ \frac{G}{n} + \frac{r_i^6 4\pi}{3\tau r_{\min}^3} \int_E^\infty \left[\int_0^\infty N(E_D, \bar{\nu}) d\bar{\nu} \right] dE_D \right\} \\ = N(E, \nu)T(E, \nu), \end{aligned} \quad (8)$$

where $T(E, \nu) = 1/\tau + 1/\tau_R + \nu + r_i^6 4\pi / (3\tau r_{\min}^3) \int_0^E g(E_A) dE_A$.

The solution of Eq. (8) is given in Appendix A. First of all, we are interested in the function $N(E, \nu)$ integrated over all quenching rates that gives the exciton distribution in energy,

$$\begin{aligned} N(E) = & \int_0^\infty N(E, \nu) d\nu \\ = & G \frac{g(E)}{n} \exp \left\{ \int_0^\infty P(\nu) \ln \left[\frac{T(\infty, \nu)}{T(E, \nu)} \right] d\nu \right\} \int_0^\infty \frac{P(\nu) d\nu}{T(E, \nu)}. \end{aligned} \quad (9)$$

The PL intensity is proportional to the total number of excitons that is obtained by integrating Eq. (9) over energy,

$$\begin{aligned} N = & \int_0^\infty N(E) dE \\ = & \frac{3G\tau r_{\min}^3}{nr_i^6 4\pi} \left(\exp \left\{ \int_0^\infty P(\nu) \ln \left[\frac{\tau\tau_R T(\infty, \nu)}{(\tau + \tau_R + \tau\tau_R \nu)} \right] d\nu \right\} - 1 \right). \end{aligned} \quad (10)$$

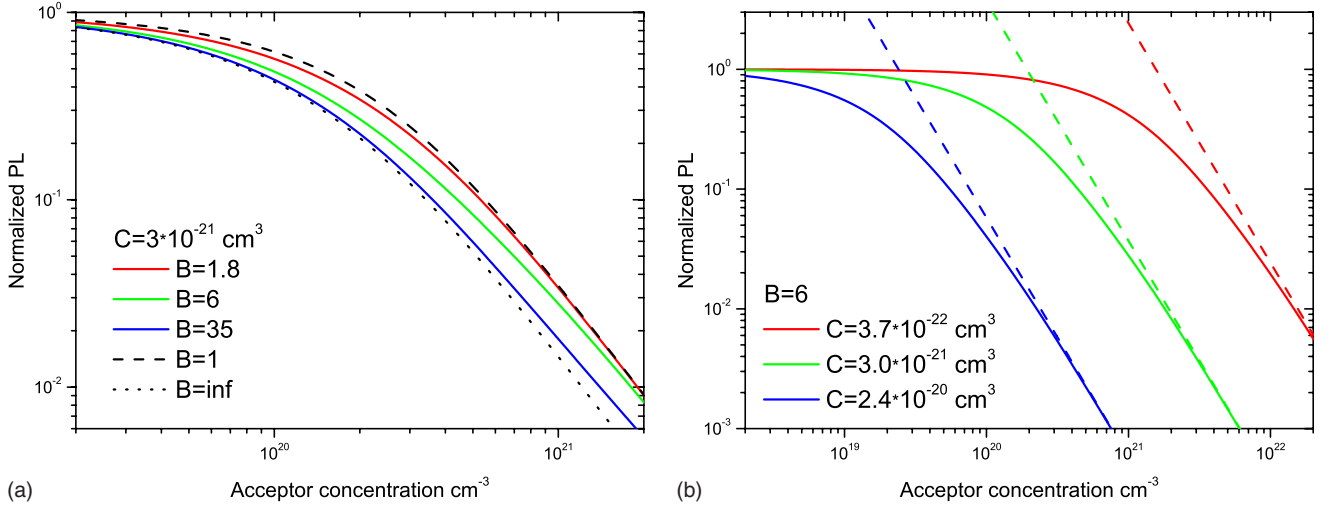


FIG. 1. (Color online) Normalized PL quenching curves. (a) PL quenching curves for different B parameters. Broken curves show the asymptotes for $B=1$ and $B \rightarrow \infty$. (b) PL quenching curves for different C parameters. Broken lines show the asymptotes at high acceptor concentration ($q \rightarrow \infty$).

Equation (10) gives the number of excitons in a blend of conjugated polymer with energy acceptors (quenchers) that quench the polymer PL via FRET. The Förster radius for the polymer-quencher interaction and the quencher concentration are parameters of the function $P(\nu)$. This function is calculated in Appendix B for the homogeneous spatial distribution of quenchers,

$$P(\nu) = \frac{2\pi q r_F^3}{3\sqrt{\tau\nu^3}} \Phi\left(\nu - \frac{16\pi^2 q^2 r_F^6}{9\tau}\right), \quad (11)$$

where Φ is the Heavyside function, r_F is the Förster radius for FRET between a polymer conjugated segment and a quencher, and q is the quencher concentration.

C. PL quenching

The dependence of exciton number N on the concentration of homogeneously distributed quenchers is given by Eq. (10) and the explicit form of $P(\nu)$ [Eq. (11)]. Introducing the following notations:

$$A = GQ\tau, \quad B^2 = \frac{4\pi r_i^6 n}{3r_{\min}^3} Q + 1, \quad C = \frac{4\pi r_F^3}{3} \sqrt{Q}, \quad (12)$$

where $Q = \tau_R / (\tau_R + \tau)$ is the PL quantum yield, one can write down the result as

$$N(q) = \frac{A}{B^2 - 1} \cdot \left(\frac{B^2 + (Cq)^2}{1 + (Cq)^2} \cdot \exp\left\{ Cq\pi \left(\frac{1}{B} - 1 \right) + 2Cq \left[\arctan(Cq) - \frac{\arctan(Cq/B)}{B} \right] \right\} - 1 \right). \quad (13)$$

The PL intensity in the blend is proportional to the exciton number N . In experiment, the normalized PL dependence on quencher concentration q is usually measured. To get this dependence, we divide Eq. (13) by the exciton number in the pristine polymer $N(0)$,

$$PL(q) = \frac{N(q)}{N(0)} = \frac{N(q)}{A}. \quad (14)$$

Equation (14) gives the two-parametric analytical expression for the PL dependence on the quencher concentration. Figure 1 shows PL quenching curves calculated from Eq. (14) for various B and C . As Eq. (12) shows, these two parameters are combinations of the four parameters characterizing the polymer (r_i , Q , n , and r_{\min}) and the one characterizing the polymer-quencher interaction (r_F). The radius r_F can be calculated if the polymer PL quantum yield Q is known. To calculate r_i , one also needs to specify the density of conjugated segments n , and the distance r_{\min} between them can be estimated as $r_{\min} = n^{-1/3}$. The values of parameter B in Fig. 1(a) correspond to $r_i = 0.7, 1.1, \text{ and } 2$ nm assuming that $r_F = 1$ nm, $Q = 0.5$, $n = 2 \times 10^{21} \text{ cm}^{-3}$, and $r_{\min} = 0.6$ nm. The values of parameter C in Fig. 1(b) correspond to $r_F = 0.5, 1, \text{ and } 2$ nm assuming that $r_i = 1.1$ nm and the rest of parameters are the same. As follows from Fig. 1(a), the PL quenching dependence on B is relatively weak. At the same time, the PL quenching dependence on C determined mostly by the Förster radius r_F of energy transfer from the conjugated segments to the quenchers [see Eq. (12)] is relatively strong (Fig. 1(b)).

The asymptote of the PL quenching curve at high quencher concentration can be easily obtained from Eq. (13),

$$N(q) \xrightarrow{q \rightarrow \infty} \frac{A}{3(Cq)^2} + o\left(\frac{1}{q^2}\right). \quad (15)$$

The asymptotes for several C are depicted in Fig. 1(b).

One can also get the asymptotic approximation of Eq. (13) when FRET between the conjugated segments is either absent ($r_i = 0$) or extremely efficient ($r_i \rightarrow \infty$). In the former case ($B = 1$), we have

$$N(q) \xrightarrow{B \rightarrow +1} A \left\{ 1 - Cq \left[\frac{\pi}{2} - \text{atan}(Cq) \right] \right\} + o(B-1). \quad (16)$$

In the latter case ($B \rightarrow \infty$), we obtain

$$N(q) \xrightarrow{B \rightarrow \infty} \frac{A \exp[2Cq(\text{atan}(Cq) - \pi/2)]}{1 + (Cq)^2}. \quad (17)$$

The asymptotes for $B=1$ and $B \rightarrow \infty$ are shown in Fig. 1(a). Combining Eqs. (16) and (17), we get the maximum contribution of FRET between the conjugated segments into PL quenching,

$$\max_{q \in [0, \infty)} \left(\frac{\lim_{B \rightarrow \infty} [N(q)]}{\lim_{B \rightarrow +1} [N(q)]} \right) = \frac{3}{e^2} \approx 0.4. \quad (18)$$

As a result, the exciton migration via intrapolymer FRET can increase the quenching efficiency up to $\sim 60\%$.

III. EXPERIMENTAL

To check the above model, we studied PL quenching in blends of an archetypical luminescent conjugated polymer poly[2-methoxy-5-(2-ethyl-hexyloxy)-1,4-phenylene vinylene] (MEH-PPV) with low-molecular-weight acceptor 2,4,7-trinitrofluorenone (TNF). The MEH-PPV (5 g/l) and TNF (≤ 0.5 g/l) were dissolved separately in chlorobenzene. Then the solutions were mixed with molar ratios MEH-PPV:TNF ranging from 1:0.0001 to 1:0.4 per monomer. Blend and reference MEH-PPV pristine films were deposited on glass substrates by drop- and spin-casting at 1300 rpm from the same solution. Drop- and spin-casting methods provide very different times of solvent evaporation during the film formation that can influence possible acceptor aggregation (i.e., the acceptor distribution in the polymer). To check possible aggregation effects on PL quenching, the two methods of film preparation were used.

PL was measured in the backscattering geometry under ambient conditions. The PL signal was dispersed using a monochromator with additional filters and was recorded using a Si detector and a lock-in amplifier. The samples were excited at a wavelength of 532 nm with a maximum intensity of 50 mW/cm^2 . The shapes of all the PL spectra were identical excluding the sample with the highest TNF content (1:0.4), for which the PL was below the noise level. The PL intensity was measured at the maximum of MEH-PPV PL (at 600 nm) in several spots on each sample with subsequent averaging. The optical thickness of the spin-cast films was about unity, and the PL data were corrected to their optical absorption at the pump wavelength. As the drop-cast films were optically thick at this wavelength, the PL data are given without such a correction. To take into account the possible photodegradation effect during recording the PL spectra, we recorded a set of PL spectra successively and compared them. The photodegradation affected the PL intensity by no more than 10%–15% for pristine MEH-PPV films, which are most prone for the effect. For the blends, the photodegradation rate was decreased together with the PL.²²

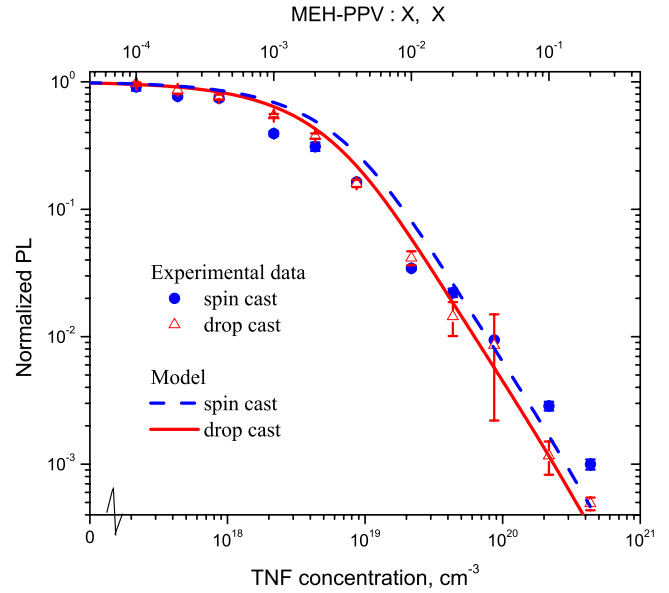


FIG. 2. (Color online) Normalized PL in MEH-PPV/TNF blends as a function of acceptor concentration for films prepared by spin casting (circles) and drop-casting (triangles). Curves are fits according to Eq. (14) with parameters $B=20 \pm^{30}_{19}$, $C=(7.3 \pm 1.2) \times 10^{-20} \text{ cm}^3$ for drop-cast (solid), and $B=19 \pm^{58}_{18}$, $C=(6 \pm 2.1) \times 10^{-20} \text{ cm}^3$ for spin-cast films (dashed).

IV. COMPARISON WITH EXPERIMENTAL DATA

To compare the above model with experiment, we have recorded PL quenching curves in MEH-PPV/TNF blend films. In these blends, a charge-transfer complex (CTC) between MEH-PPV and TNF is formed in the electronic ground state.^{16,17} This CTC has considerable absorption in the MEH-PPV optical gap that results in good spectral overlapping of the polymer PL and CTC absorption spectra. Therefore, the CTC can be an efficient energy acceptor (quencher) collecting the excitons via FRET from the photoexcited MEH-PPV conjugated segments.

Figure 2 compares the experimental and model data on PL quenching in MEH-PPV/TNF blends. The data are presented for two different film preparation methods: drop- and spin-casting. Both experimental curves are quite similar in a dynamic range of 1000 regardless very different evaporation times during the solidification. This similarity can be a result of a more or less homogenous acceptor distribution in the films. This suggestion is in accordance with the light scattering²³ and Raman²⁴ data on MEH-PPV/TNF blend films.

To obtain the Förster radii r_i and r_F from fitting parameters B and C , respectively, we need to specify the other parameters in Eq. (12). We used the experimentally measured PL quantum yield in MEH-PPV drop-cast films $Q=0.2$ (Ref. 25) and suggested that the average MEH-PPV conjugated segment length is five polymer units.²⁶ As a result, we have $n=4.5 \times 10^{20} \text{ cm}^{-3}$ taking the film density as 1 g/cm^3 . The minimal distance between MEH-PPV conjugated segments $r_{\min}=0.4 \text{ nm}$ is taken from the x-ray data.^{27,28} Accordingly, we obtain the radii $r_i=2.0 \pm 1$ and $r_F=3.4 \pm 0.1 \text{ nm}$ for intrapolymer and polymer-quencher

FRET, correspondingly, for the drop-cast films. We give the Förster radii only for the drop-cast films as the fitting accuracy for them is better than for the spin-cast ones (Fig. 2).

One can compare the polymer-quencher Förster radius r_F derived from fitting with that calculated from the overlapping of the MEH-PPV PL and quencher (CTC) absorption spectra according to Eq. (1). Using the MEH-PPV/TNF CTC absorption spectrum from Ref. 29 and the refraction index spectrum for MEH-PPV from Ref. 30, we calculated the polymer-quencher Förster radius $r_F=3.5$ nm. Therefore, the two r_F obtained from the direct calculation and fitting are in excellent agreement.

In addition, we have applied our model to the experimental data on PL quenching in blends of phenyl-substituted polyphenylenevinylene (PhPPV) and TNF.³¹ The experimental quenching curve (Fig. 8 in Ref. 31) is very similar in shape to those plotted in Fig. 2. The presence of the CTC as a quencher of the polymer PL in PhPPV/TNF blends is expected similar to that observed in MEH-PPV/TNF blends.¹⁶ Indeed, the CTC can be identified as a feature in the photocurrent spectra of PhPPV/TNF blends.³¹ We have found that the model curve according to Eq. (14) excellently fits the PL quenching data in the PhPPV/TNF blends with $B=1\pm 0.9$ and $C=(5.2\pm 0.8)\times 10^{-20}$ cm⁻³. Using $Q=0.4$,³¹ we obtain the polymer-quencher Förster radius $r_F=2.7\pm 0.1$ nm. Note that the approximation error for parameter B was too large to estimate the intrapolymer Förster radius r_i .

V. DISCUSSION

Our model gives the steady-state energy distribution of excitons [Eq. (9)] of a conjugated polymer blended with energy acceptors. Integration of Eq. (9) over energy gives the total number of excitations [Eq. (10)], which is independent on the energy density of excitonic states $g(E)$. It is well known that acceptor molecules are prone to aggregation in the polymer matrix.³² The spatial distribution of acceptor in our model is taken into account by the function $P(\nu)$ that allows the model to be adapted to different acceptor distributions in the blend. Specifically, phase separated donor-acceptor blends could be modeled. In the simplest case of the homogeneous acceptor distribution, the PL quenching curve is expressed in the elementary functions [Eq. (13)].

The normalized PL quenching curve [Eq. (14)] contains the only two fitting parameters B and C . As Eq. (12) shows, the former is related to the Förster radius of the intrapolymer energy transfer (r_i), the PL quantum yield, and a volume per one conjugated segment. The latter depends only on the energy transfer radius from a conjugated segment to the quencher (r_F) and the PL quantum yield. In the case of unit PL quantum yield, the B and C parameters can be associated with volumes corresponding to r_i and r_F , respectively [Eq. (12)]. In fact, the C parameter is the volume of a ball with radius r_F , and the B parameter (if $B\gg 1$) is proportional to the volume of a ball with radius r_i normalized to the characteristic volume occupied by a conjugated segment.

Equation (14) has the simple asymptotes at high acceptor concentration [Eq. (15)] and also at $r_i=0$ [Eq. (16)] and $r_i\rightarrow\infty$ [Eq. (17)]. The latter asymptotes allowed us to find the

maximum contribution of intrapolymer FRET into PL quenching [see Eq. (18)] amounting $\sim 60\%$. At the same time, change in the Förster radius r_F only by two times (see Fig. 1) changes the PL intensity by two orders of magnitude. The explanation of this different sensitivity of PL quenching to r_F and r_i is straightforward. As follows from Eq. (3), increase in the r_F by n times enhances the quenching rate by n^6 times, whereas any increase in the r_i results mainly in more efficient migration of excitons. The latter does increase the PL quenching efficiency but only for a small part of excitons located farther than r_F from the quenchers.

Application of our model to the experimental PL quenching data on PhPPV/TNF blends from Ref. 31 and our data on MEH-PPV/TNF blends gives excellent agreement: the two-parametric closed-form expression closely follows the measured PL quenching curve over a dynamic range more than three orders of magnitude. The polymer-quencher Förster radius derived from the fit is $r_F=2.7\pm 0.1$ nm in the PhPPV/TNF blends and $r_F=3.4\pm 0.1$ nm in the MEH-PPV/TNF blends. This difference in r_F corresponds a higher PL quenching efficiency observed for MEH-PPV (Fig. 2) as compared to PhPPV (Fig. 8 in Ref. 31). Possibly, the CTC, as an energy acceptor, in the PhPPV/TNF blends is less pronounced than in the MEH-PPV/TNF blends due to bulkier side groups of PhPPV.

Remarkably, the r_F for the MEH-PPV/TNF blends perfectly matches the FRET radius calculated from the spectral overlapping according to Eq. (1). This correspondence of the two FRET radii confirms the usefulness of our model in spite of its severe approximations (see below). The intrapolymer FRET radius in the MEH-PPV/TNF blends was estimated to be $r_i=2.5\pm 1.2$ nm. Note that the fitting accuracy of r_i is far worse than that of r_F (Fig. 2). This is explained by weak PL quenching dependence on the intrapolymer FRETs [see Fig. 1(a)] that is comparable to the experimental error.

Note that the same PL quenching data on PhPPV/TNF blends were also described by the sphere-of-action model.³³ In this model, an exciton has a constant quenching rate when it approaches to a quencher closer than a quenching radius r_q during migration. The $r_q=1.4$ nm was obtained in Ref. 33 that is far less than the r_F . However, the r_F and r_q should not be compared as they correspond to the different quenching models.

As mentioned in the introduction section, the model of Arkhipov *et al.* (Ref. 12) can also be used to describe the steady-state PL quenching in doped conjugated polymers via FRET to energy acceptor. That model describes the PL kinetics, and its steady-state solution needs numerical integration over time. On the other hand, our model has initially been formulated in the steady state. Using assumptions (i–vi) similar to those of Arkhipov *et al.* (Ref. 12), the model allows the closed-form exact solution giving the PL quenching curve depending on the two parameters B and C [Eq. (14)]. Thus, the key advantage of our model is that allows fitting experimental data on cw PL quenching by the two-parametric analytical expression [Eq. (14)]. In addition, our model can be extended to take into account acceptor aggregation that is typical for blends with high acceptor content. This extension can be done by a modification of the probability distribution on quenching rate $P(\nu)$.

An important PL quenching process that is not included in the model is charge transfer to an electron acceptor. In blends of conjugated polymers and fullerenes, it is usually believed that photoinduced charge transfer results in PL quenching.³⁴ Photoinduced charge transfer can be included in our model by constructing an appropriate quenching rate density function $P(\nu)$ taking into account both quenching probabilities, i.e., via FRET and photoinduced charge transfer.

Now discuss the assumptions of our model presented in Sec. II. We suggested that spatial exciton migration results only from FRET. Nevertheless, excitons could also move via Dexter energy transfer between the conjugated segments.³⁵ The Dexter energy transfer is short-ranged as compared to the FRET as the former needs overlapping of the molecular orbitals of conjugated segments. Therefore, the Dexter mechanism is expected to result in small underestimating of exciton migration. The latter could possibly be taken into account by a small effective increase in the intrapolymer FRET.

We assumed above that FRET occurs between point dipoles (vi). However, excitons in conjugated polymers can be delocalized over a number of repeat units that could influence FRET. Exciton delocalization can be taken into account by several ways, e.g., by using the linear dipoles approach³⁶⁻³⁸ or the transition density approach.³⁹ If the characteristic exciton delocalization length is shorter than the intrapolymer Förster radius, the exciton delocalization is expected to be ineffective. Otherwise, the point-dipole approximation can result in underestimation or overestimation of the intrapolymer Förster radius depending on the mutual orientation of the conjugated segments.⁴⁰ These deviations are likely to be cancelled out in amorphous polymer films that can explain very good agreement of our model with the experimental data.

The low-temperature approximation (iv) prohibits any increase in the exciton energy resulting from the intrapolymer FRET. This approximation results in neglect of the quasi isoenergetic exciton migration in the polymer after the fast downhill energy transfer.⁴¹ Nevertheless, the rate of downhill FRET during the initial exciton relaxation⁴¹ and subsequent quenching can be much faster than the isoenergetic transfer rate. To fulfill this condition, it is sufficient to have the typical width of exciton energy distribution $g(E)$ considerably larger than the characteristic thermal energy kT . This condition is usually fulfilled in conjugated polymers.

We assumed above that all the conjugated segments have the same absorption cross-section at the photoexcitation wavelength (ii). On one hand, it is well known that the absorption and PL spectra of conjugated chains depend on their length. On the other hand, these spectra are usually considerably broadened due to strong electron-vibrational coupling. This broadening can weaken the absorption cross-section dependence on the conjugated length and on the photoexcitation wavelength. This feature of polymer conjugated chains justifies assumption (ii). Moreover, it substantiates using the effective Förster radii r_i and r_F instead of the corresponding distributions in them.

VI. CONCLUSION

We have developed an analytical model describing the steady-state PL quenching via FRET in homogeneous blends

of a conjugated polymer and energy acceptor molecules. The model can also be extended to the more complicated cases of phase separated polymer-acceptor blends. Spatial and energy migration of excitons stemming from the multichromophoric structure of the conjugated polymer are taken into account in the model. Importantly, the model has the only two fitting parameters associated with the intrapolymer and polymer-acceptor FRET radii. The model predicts that the intrapolymer FRET can enhance the PL quenching up to 60%. Comparison of the model to the experimental data in blends of soluble polyphenylenevinylenes and a low-molecular-weight electron acceptor resulted in very good agreement indicating that the model can be a useful and simple tool for data analysis on steady-state PL quenching in polymer-acceptor blends.

ACKNOWLEDGMENTS

This work is supported by Russian Foundation for Basic Research (Grant No. 07-02-01227-a). We thank E. V. Emelianova for helpful discussions.

APPENDIX A

The solution of Eq. (8) can be obtained by introducing the new sought function $R(E, \nu)$

$$N(E, \nu) = g(E)P(\nu)R(E, \nu) \quad (\text{A1})$$

and subsequent differentiation of Eq. (8) by ν . As a result, we get the linear differential homogeneous equation,

$$\frac{\partial R(E, \nu)}{\partial \nu} T(E, \nu) + R(E, \nu) = 0, \quad (\text{A2})$$

where $T(E, \nu)$ is defined in Eq. (8). The solution of Eq. (A2) is known accurate to a function $X(E)$,

$$R(E, \nu) = \frac{X(E)}{T(E, \nu)}. \quad (\text{A3})$$

Substituting the solution in the initial equation [Eq. (8)] and differentiating it by E , we get a linear homogeneous differential equation,

$$X'(E) + \frac{r_i^6 4\pi}{3\tau r_{\min}^3} g(E)X(E) \int_0^\infty \frac{P(\nu)}{T(E, \nu)} d\nu = 0. \quad (\text{A4})$$

Using relations between $N(E, \nu)$ and $R(E, \nu)$ [Eq. (A1)] and between $R(E, \nu)$ and $X(E)$ [Eq. (A3)] and then applying them to the solution of Eq. (A4), we can obtain function $N(E, \nu)$ accurate to some constant C ,

$$N(E, \nu) = C \frac{g(E)P(\nu)}{T(E, \nu)} \times \exp \left\{ - \int_0^\infty P(\nu) \ln \left[\frac{T(E, \nu)}{1/\tau + 1/\tau_R + \nu} \right] d\nu \right\}. \quad (\text{A5})$$

The constant C is found by substitution the solution (A5) into the initial equation [Eq. (8)],

$$C = \frac{G}{n} \exp \left\{ \int_0^\infty P(\nu) \ln \left[\frac{T(\infty, \nu)}{1/\tau + 1/\tau_R + \nu} \right] d\nu \right\}. \quad (\text{A6})$$

The final form of $N(E, \nu)$ can be found by substituting Eq. (A6) into Eq. (A5),

$$N(E, \nu) = G \frac{g(E)}{n} \frac{P(\nu)}{T(E, \nu)} \exp \left\{ \int_0^\infty P(\nu) \ln \left[\frac{T(\infty, \nu)}{T(E, \nu)} \right] d\nu \right\}. \quad (\text{A7})$$

APPENDIX B

Each exciton can be characterized by a quenching rate via FRET to the energy acceptor. This rate depends on the exciton position relative to the acceptors. For any exciton position, there is a probability density function $P(\nu)$ to have the quenching rate ν . To obtain $P(\nu)$, one must find for each ν a corresponding phase-space density of acceptor coordinates in

which the quenching rate is in the range $[\nu, \nu + d\nu]$, divide it by $d\nu$, and then normalize the result to the whole phase-space volume. One can find $P(\nu)$ by finding the primitive of $P(\nu)$ and its subsequent differentiation.

To build a probability density function $P(\nu)$ for homogeneously distributed acceptor quenching the PL via FRET, we consider a solid sphere with radius R . Then we put an exciton in the sphere center and n acceptors randomly distributed in the sphere. The acceptor concentration q is

$$q = \frac{3}{4\pi} \frac{n}{R^3}. \quad (\text{B1})$$

We denote the primitive of $P(\nu)$ in the sphere by $F_n(\nu, R)$. To find $F_n(\nu, R)$, we need to calculate the normalized phase-space density of acceptors coordinates where the quenching rate is less than ν . This function is then described by the integral of the Heavyside function over all acceptor coordinates normalized on the whole phase-space volume,

$$F_n(\nu, R) = \frac{1}{(4\pi/3R^3)^n} \cdot \underbrace{\int_0^{2\pi} \int_{-\pi/2}^{\pi/2} \int_0^R \cdots \int_0^{2\pi} \int_{-\pi/2}^{\pi/2} \int_0^R}_{n} \Phi \left(\nu - \sum_{i=1}^n \frac{r_i^6}{\tau r_i} \right) r_1^2 \sin(\theta_1) dr_1 d\theta_1 d\varphi_1 \cdots r_n^2 \sin(\theta_n) dr_n d\theta_n d\varphi_n, \quad (\text{B2})$$

where Φ is the Heavyside function determining whether the quenching rate is less than ν ; and r_m, θ_m, φ_m are the m -th acceptor spherical coordinates. Integrating over the angular coordinates and denoting r_m^6 as x_m , we can simplify Eq. (B2),

$$F_n(\nu, R) = \frac{1}{(2R^3)^n} \underbrace{\int_0^{R^6} \cdots \int_0^{R^6}}_n \Phi \left(\nu - \sum_{i=1}^n \frac{r_i^6}{\tau x_i} \right) d\sqrt{x_1} \cdots d\sqrt{x_n}. \quad (\text{B3})$$

Now we isolate the n th acceptor in the Heavyside function,

$$\Phi \left(\nu - \sum_{i=1}^n \frac{r_i^6}{\tau x_i} \right) = \Phi \left(\nu - \sum_{i=1}^{n-1} \frac{r_i^6}{\tau x_i} \right) \Phi \left(x_n - \frac{1}{\frac{\tau \nu}{r_F^6} - \sum_{i=1}^{n-1} \frac{1}{x_i}} \right). \quad (\text{B4})$$

The Heavyside function in the integrand of Eq. (B3) only limits the integration range. Using the identity

$$\int_a^b \Phi(x-c) f(x) dx \equiv \int_c^b f(x) dx \cdot \Phi(b-c), \quad c > a \quad (\text{B5})$$

and Eqs. (B4) and (B5), it is possible to take the modified Heavyside function out from the last integral in Eq.(B3),

$$F_n(\nu, R) = \frac{1}{2^n R^{3n}} \underbrace{\int_0^{R^6} \cdots \int_0^{R^6}}_{n-1} \Phi \left(\nu - \sum_{i=1}^{n-1} \frac{r_i^6}{\tau x_i} \right) \int_{\frac{\tau \nu}{r_F^6} - \sum_{i=1}^{n-1} \frac{1}{x_i}}^{R^6} \frac{1}{\sqrt{x_n} \sqrt{x_1} \cdots \sqrt{x_{n-1}}} dx_n, \quad (\text{B6})$$

where

$$\nu_i = \nu - i \frac{r_F^6}{\tau R^6}. \quad (\text{B7})$$

Comparing the initial Eq. (B3) and modified Eq. (B6), one can notice that this operation can be repeated until the Heavyside function leaves the integrand,

$$F_n(\nu, R) = \frac{\Phi(\nu_n)}{2^n R^{3n}} \int_{\frac{\tau\nu_{n-1}}{r_F^6}}^{R^6} \frac{1}{\frac{\tau\nu_{n-2}}{r_F^6} - \sum_{i=1}^{n-1} \frac{1}{x_i}} \dots \int_{\frac{\tau\nu_1}{r_F^6} - \sum_{i=1}^{n-2} \frac{1}{x_i}}^{R^6} \frac{1}{\frac{\tau\nu_0}{r_F^6} - \sum_{i=1}^{n-1} \frac{1}{x_i}} \int_{\frac{\tau\nu_0}{r_F^6} - \sum_{i=1}^{n-1} \frac{1}{x_i}}^{R^6} \frac{1}{\frac{\tau\nu_0}{r_F^6} - \sum_{i=1}^{n-1} \frac{1}{x_i}} \times \frac{dx_1}{\sqrt{x_1}} \dots \frac{dx_n}{\sqrt{x_n}}. \quad (\text{B8})$$

Supposing that $\nu_2 \rightarrow \nu_0$ at $R \rightarrow \infty$, one can get the function $F_n(\nu, R)$,

$$F_n(\nu, R) = \left(1 - \frac{nr_F^3}{R^3 \tau \sqrt{\nu_n}} \right) \Phi(\nu_{n^2}). \quad (\text{B9})$$

We get rid of R and n by taking the limit $R \rightarrow \infty$ and using the concentration q according to Eq. (B1). Differentiating the result by ν , we get the function $P(\nu)$,

$$P(\nu) = \frac{\partial F(\nu)}{\partial \nu} = \frac{2\pi q r_F^3}{3\sqrt{\tau\nu^3}} \Phi\left(\nu - \frac{16\pi^2 q^2 r_F^6}{9\tau}\right). \quad (\text{B10})$$

-
- ¹Y. Zaushitsyn, K. G. Jespersen, L. Valkunas, V. Sundstrom, and A. Yartsev, *Phys. Rev. B* **75**, 195201 (2007).
- ²T. Q. Nguyen, I. B. Martini, J. Liu, and B. J. Schwartz, *J. Phys. Chem. B* **104**, 237 (2000).
- ³I. B. Martini, A. D. Smith, and B. J. Schwartz, *Phys. Rev. B* **69**, 035204 (2004).
- ⁴Y. V. Romanovskii, V. I. Arkhipov, and H. Bassler, *Phys. Rev. B* **64**, 033104 (2001).
- ⁵D. D. C. Bradley and R. H. Friend, *J. Phys.: Condens. Matter* **1**, 3671 (1989).
- ⁶Z. D. Popovic, *J. Chem. Phys.* **76**, 2714 (1982).
- ⁷M. Deussen, M. Scheidler, and H. Bassler, *Synth. Met.* **73**, 123 (1995).
- ⁸M. Deussen, P. Haring Bolivar, G. Wegmann, H. Kurz, and H. Bassler, *Chem. Phys.* **207**, 147 (1996).
- ⁹V. Gulbinas, Y. Zaushitsyn, V. Sundstrom, D. Hertel, H. Bassler, and A. Yartsev, *Phys. Rev. Lett.* **89**, 107401 (2002).
- ¹⁰H. D. Burrows, J. S. de Melo, C. Serpa, L. G. Arnaut, M. D. Miguel, A. P. Monkman, I. Hamblett, and S. Navaratnam, *Chem. Phys.* **285**, 3 (2002).
- ¹¹K. H. Lee, R. A. J. Janssen, N. S. Sariciftci, and A. J. Heeger, *Phys. Rev. B* **49**, 5781 (1994).
- ¹²V. I. Arkhipov, E. V. Emelianova, and H. Bassler, *Phys. Rev. B* **70**, 205205 (2004).
- ¹³J. Klafter and A. Blumen, *Chem. Phys. Lett.* **119**, 377 (1985).
- ¹⁴U. Lemmer, A. Ochse, M. Deussen, R. F. Mahrt, E. O. Gobel, H. Bassler, P. Haring Bolivar, G. Wegmann, and H. Kurz, *Synth. Met.* **78**, 289 (1996).
- ¹⁵Y. X. Liu, M. A. Summers, S. R. Scully, and M. D. McGehee, *J. Appl. Phys.* **99**, 093521 (2006).
- ¹⁶A. A. Bakulin *et al.*, *Synth. Met.* **147**, 221 (2004).
- ¹⁷D. Y. Parashchuk, S. G. Elizarov, A. N. Khodarev, A. N. Shchegolikhin, S. A. Arnautov, and E. M. Nechvolodova, *JETP Lett.* **81**, 467 (2005).
- ¹⁸A. I. Burshtein, *Usp. Fiz. Nauk* **143**, 553 (1984).
- ¹⁹T. Forster, *Discuss. Faraday Soc.* **27**, 7 (1959).
- ²⁰H. Wiesenhofer, E. Zojer, E. J. W. List, U. Scherf, J. L. Bredas, and D. Beljonne, *Adv. Mater.* **18**, 310 (2006).
- ²¹G. D. Scholes, *Annu. Rev. Phys. Chem.* **54**, 57 (2003).
- ²²I. V. Golovnin, A. A. Bakulin, S. A. Zapunidy, E. M. Nechvolodova, and D. Y. Parashchuk, *Appl. Phys. Lett.* **92**, 243311 (2008).
- ²³S. G. Elizarov, A. E. Ozimova, D. Y. Parashchuk, S. A. Arnautov, and E. M. Nechvolodova, *Proc. SPIE* **6257**, 293 (2006).
- ²⁴V. V. Bruevich, T. S. Makhmutov, S. G. Elizarov, E. M. Nechvolodova, and D. Y. Parashchuk, *J. Chem. Phys.* **127**, 104905 (2007).
- ²⁵S. A. Arnautov, E. M. Nechvolodova, A. A. Bakulin, S. G. Elizarov, A. N. Khodarev, D. S. Martyanov, and D. Y. Parashchuk, *Synth. Met.* **147**, 287 (2004).
- ²⁶T. P. Nguyen, V. H. Tran, P. Destruel, and D. Oelkrug, *Synth. Met.* **101**, 633 (1999).
- ²⁷C. Y. Yang, F. Hide, M. A. Diaz-Garcia, A. J. Heeger, and Y. Cao, *Polymer* **39**, 2299 (1998).
- ²⁸U. Jeng *et al.*, *Macromolecules* **38**, 6566 (2005).
- ²⁹O. D. Parashchuk, A. Y. Sosorev, V. V. Bruevich, and D. Y. Parashchuk (unpublished).
- ³⁰M. Tammer and A. P. Monkman, *Adv. Mater.* **14**, 210 (2002).
- ³¹C. Im, J. M. Lupton, P. Schouwink, S. Heun, H. Becker, and H. Bassler, *J. Chem. Phys.* **117**, 1395 (2002).
- ³²L. H. Nguyen, H. Hoppe, T. Erb, S. Gunes, G. Gobsch, and N. S. Sariciftci, *Adv. Funct. Mater.* **17**, 1071 (2007).
- ³³V. I. Arkhipov and H. Bassler, *Phys. Status Solidi A* **201**, 1152 (2004).
- ³⁴N. S. Sariciftci, L. Smilowitz, A. J. Heeger, and F. Wudl, *Science* **258**, 1474 (1992).
- ³⁵D. L. Dexter, *J. Chem. Phys.* **21**, 836 (1953).
- ³⁶S. Westenhoff, C. Daniel, R. H. Friend, C. Silva, V. Sundstrom, and A. Yartsev, *J. Chem. Phys.* **122**, 094903 (2005).
- ³⁷M. M. L. Grage, P. W. Wood, A. Ruseckas, T. Pullerits, W.

- Mitchell, P. L. Burn, I. D. W. Samuel, and V. Sundstrom, J. Chem. Phys. **118**, 7644 (2003).
- ³⁸S. Westenhoff, W. J. D. Beenken, A. Yartsev, and N. C. Greenham, J. Chem. Phys. **125**, 154903 (2006).
- ³⁹W. J. D. Beenken and T. Pullerits, J. Chem. Phys. **120**, 2490 (2004).
- ⁴⁰H. Wiesenhofer, D. Beljonne, G. D. Scholes, E. Hennebicq, J. L. Bredas, and E. Zojer, Adv. Funct. Mater. **15**, 155 (2005).
- ⁴¹I. G. Scheblykin, A. Yartsev, T. Pullerits, V. Gulbinas, and V. Sundstrom, J. Phys. Chem. B **111**, 6303 (2007).